Ultrafast Laser Driven Micro-Lens to Focus and Energy Select MeV Protons

Toma Toncian, Marco Borghesi, Julien Fuchs, Emmanuel d'Humières, Patrizio Antici, Patrick Audebert, Erik Brambrink, Carlo A Cecchetti, Ariane Pipahl, Lorenzo Romagnani, et al.

Ultrafast Laser Driven Micro-Lens to Focus and Energy Select MeV Protons

Toma Toncian[1], Marco Borghesi[2], Julien Fuchs[3], Emmanuel d'Humières[3,4], Patrizio Antici[3], Patrick Audebert[3], Erik Brambrink[3], Carlo Alberto Cecchetti[2], Ariane Pipahl[1] Lorenzo Romagnani[2], Oswald Willi[1].

1. *Heinrich Heine Universität Düsseldorf, D-40225 Düsseldorf, Germany*
2. *School of Mathematics and Physics, The Queen's University Belfast, Belfast BT7 1NN, Northern Ireland, United Kingdom*
3. *Laboratoire pour l'Utilisation des Lasers Intenses, UMR 7605 CNRS-CEA-Ecole Polytechnique-Université Paris VI, 91128 Palaiseau, France*
4. *Centre de Physique Théorique, UMR 7644 CNRS-Ecole Polytechnique, 91128 Palaiseau, France*

Abstract:

We present a technique for simultaneous focusing and energy selection of high-current, MeV proton beams using radial, transient electric fields (10^7-10^{10} V/m) triggered on the inner walls of a hollow micro-cylinder by an intense, subpicosecond laser pulse. Due to the transient nature of the focusing fields, the proposed method allows selection of a desired range out of the spectrum of the poly-energetic proton beam. This technique addresses current drawbacks of laser accelerated proton beams, i.e. their broad spectrum and divergence at the source.

The recent development of ultra-intense laser pulses (*1*) has opened up opportunities for applications in many areas including particle acceleration (*2-5*) inertial fusion energy (*6*), generation of intense x-ray pulses (*7*), laser-driven nuclear physics (*8*) and laboratory astrophysics (*9*). In particular, the acceleration of MeV ions from the interaction of high-intensity laser-pulses with thin solids has major applicative prospects due to the high beam quality of these ion bursts (*10,11*). Such proton beams are already applied to produce high energy density matter (*12*) or to radiograph transient processes (*13*), and offer high prospects for tumour therapy (*14*), isotope generation for positron emission tomography (*15*), fast ignition of fusion cores (*16*), and brightness increase of conventional accelerators. However, as these proton beams are poly-energetic and divergent at the source, reduction and control of their divergence and energy spread are essential requirements for most of these applications.

Focusing of energetic proton beams is usually achieved using electrostatic or magnetic lenses (*17*) that have several drawbacks, namely: slow switching times, large sizes, asymmetry in the transverse plane for the focused beam, aberrations, inability to focus large currents, and large heat dissipation. It has been proposed that particle selection and beam collimation of laser produced protons applicable for tumour therapy could be achieved by means of superconducting magnet systems (*18*). Relativistic laser-plasma devices appear in principle more suitable to achieve the required angular and spectral control of laser-accelerated ion beams since they can withstand large ion beam currents, can be switched over ps time scales, and can support large deflecting fields on micro-scales.

Advances in ion beam tailoring have been achieved so far mainly by employing target engineering techniques. Geometrical focusing of laser-driven protons has been attained by using curved targets (*12*). Demonstration of this technique has been limited so far to focal distances of a few mm, and to the low energy component of the proton spectrum. Very recently, quasi-monochromatic acceleration from laser irradiated micro-structured targets has been reported (*19,20*). In these approaches, the focusing or energy selection effect is achieved by directly acting on the source. As a consequence, these techniques rely on relatively complex target fabrication or preparation procedures.

We describe here an alternative approach which provides tuneable, simultaneous focusing and energy selection of MeV proton beams. Furthermore, our approach decouples the beam tailoring stage from the acceleration stage allowing for their independent optimization. This leads to a system with higher flexibility than the methods above, relaxing significantly the target fabrication constraints. The method employs a compact laser driven micro-lens arrangement, a schematic of which is shown in Fig 1A. Figs 1B-C sketch the underlying physical process: relativistic electrons injected through the cylinder's wall by the CPA_2 laser pulse spread evenly on the cylinder's inner walls and initiate hot plasma expansion. The transient electric fields associated with the expansion are employed, in a radial geometry, to focus protons accelerated by the CPA_1 laser pulse from a thin planar foil. The micro-lens operation was demonstrated in experiments carried out at the LULI Laboratory, employing the 100 TW laser (*21*) operating in the

Chirped Pulse Amplification mode (CPA). After amplification, the laser pulse was split into two separate pulses (CPA_1 and CPA_2) which were recompressed in separate grating compressors to a 350 fs duration. The delay between the two pulses was controlled optically with picosecond precision. The CPA_1 pulse (irradiance $I=5x10^{19}$ W/cm^2) was used to accelerate a high-current, diverging beam of up to 15 MeV protons from a 25 μm thick Al foil target (the protons are produced from hydrocarbon impurities (*22*) on the target rear surface (*23*,*24*)). The CPA_2 pulse ($I = 3x10^{18}$ W/cm^2) was focused onto the outer wall of a hollow cylinder. The proton beam from the first foil was directed through the cylinder and detected with a stack of Radiochromic Films (RCF, a dosimetric detector (*25*)) positioned at a variable (from 2 to 70 cm) distance from the proton source. The RCF stack was used to measure the proton beam divergence. It also provided a coarse energy resolution due to the energy deposition properties of the ions (*3*) (most of the energy of a proton is released in the so-called Bragg peak, located at a distance in the detector which depends on the incident proton energy). It was shielded with an 11 μm Al foil allowing protons with energies above 1.5 MeV to be recorded. In some cases, a central mm-sized hole was bored through the RCF to allow downstream high spectral resolution measurements using a magnetic spectrometer with a 0.6 T permanent magnet. The spectral resolution determined by the slit width and the dispersion of the spectrometer is 0.2 MeV at 6 MeV and 0.7 MeV at 15 MeV. The distance between the proton production foil and cylinder and the distance between the cylinder and detector were varied throughout the experiment. At a source-cylinder distance of 1 mm the proton flux increase due to focusing by the micro-lens was so strong that saturation of the film occurred. Quantitative data could only be obtained when the cylinder was moved to 4 mm from the proton foil, in order to collect a smaller part of the diverging proton beam.

Fig. 2A shows different layers (the 5th and 6th in the stack, corresponding to protons of 9 and 7.5 MeV respectively) of an RCF pack recording the proton beam after its propagation through a laser-illuminated dural cylinder 3 mm in length, 700 μm in diameter and 50 μm in wall thickness. The entrance plane of the cylinder was placed 4 mm from the proton producing foil. The distance from the proton-producing foil to CPA_2 irradiation point on the cylinder was 5 mm. As expected, no focusing effect is observed for the 9 MeV protons. Indeed, the electric field is triggered by the CPA_2 laser pulse ~20 ps after these protons exit the cylinder. For the 7.5 MeV protons, the electric field just develops while these protons are close to exit the cylinder and a small spot about 600 μm (FWHM) in diameter is seen on the RCF at the centre of the cylinder's shadow (spots as small as 200 μm have been observed depending on the detector position). In this case the proton flux within the spot at the film plane is increased by up to 12 times compared to the unfocused part not captured by the cylinder (Fig. 2B). Based on the known properties of the proton source and on the decay time of the focusing fields (inferred to be ~ 10 ps from PIC simulations -described later- and experimental results (*26*)), a focused current of about 5 A can be estimated for the conditions of Fig.3. We have also studied the evolution of the beam size, as a function of the propagation distance from the cylinder. This was done under the same conditions of Fig 2. The behaviour of the 7.5 MeV proton component, is illustrated in Figure 3. Note that for this energy, the beam size is only 8 mm after 70 cm of propagation whereas freely propagating, the size of the beam would have been ~260 mm. Finally, Fig 4 shows the spectrum obtained, again in the same experimental configuration, using the magnetic spectrometer, with an entrance slit of 250 μm positioned 70 cm away from the proton source. As a reference, we also show a typical exponential spectrum collected in the same conditions, but without the micro-lens. The data shows clearly the energy selection capability of the micro-lens: due to selective collimation of the 6.25 MeV protons, these could be transmitted efficiently through the spectrometer slit (acting as an angular filter), and their density after the slit in the spectrally dispersed plane is enhanced as compared to the free-space expansion case. For this shot, the 6.25 MeV protons experience the focusing fields for ~5 ps before exiting the cylinder. Note that we obtain an energy spread of 0.2 MeV - limited by the spectrometer energy resolution - for the peak located at 6.25 MeV. As shown in Fig 4, the PIC simulations performed in the same conditions as in the experiment, suggest that the spectral width of the peak is around 0.1 MeV and hence narrower than demonstrated by the experimental spectrum shown. By varying the optical delay between the laser beams, the location of this peak on the energy axis can be tuned selectively (as demonstrated experimentally), therefore allowing

to tailor the energy distribution of the transmitted beam, a necessary step for many of the applications mentioned earlier. We would like to emphasize that with this approach focusing and energy selection are provided simultaneously.

1D and 2D Particle-in-Cell (PIC) simulations of field generation at the micro-lens' walls and 3D test-particle simulations of proton propagation through the micro-lens were performed. The simulations were performed in three steps using the CALDER code *(27)*. First, we verified, using 2D simulations that the laser pulse triggering the micro-lens by irradiating the cylinder's outer wall, generated a population of hot electrons that spread evenly on the cylinder's walls. We then used a 1D code to simulate the plasma expansion within the cylinder, i.e. we simulated the expansion of 2 slabs of plasma separated by 700 μm (the cylinder's diameter). The expansion is driven by a hot electron population having a Boltzmann distribution with a temperature of 400 keV as given by the ponderomotive potential at the irradiance of CPA_2 (*28*). The initial electron density at the cylinder's wall is estimated by considering that a 40 % (inferred from experimental measurements (*29*)) fraction of the laser energy is converted into hot electrons and then that these are spread evenly on the cylinder's walls. This results in a hot electron density of $\sim 6\times10^{16}$ cm^{-3}. We assume that when the plasma expansion starts, the field obtained in the PIC simulation is the same along the whole cylinder. Finally we simulate the propagation of a proton beam in the cylinder, through the space and time dependent fields obtained from the PIC simulation. The proton source used in the simulations has a divergence and energy spectrum as measured in the experiment.

The successful comparison between the simulations and the data, as shown in Figs 3 and 4 supports the above mentioned scenario in which laser-triggered transient fields drive the selective deflection of the protons. The transient field (*30*) is associated with a hot electron sheath that extends over a Debye length ahead of the plasma, expanding toward the cylinder's axis (*26,31*). The different energy components present in the proton beam spectrum transit through the cylinder at different times due to their different velocities, with higher energy protons crossing the cylinder at earlier times. Protons passing through the micro-lens before it is triggered (as in Fig 2A for the 9 MeV layer), do not experience any fields and are therefore not deflected. Protons which are crossing the cylinder and are close to its end when it is triggered, and therefore experience the fields for only a short time, will exit the cylinder with a very low divergence (as in Fig 2A for the 7.5 MeV layer). Lower energy protons will experience a larger cumulated field along their propagation through the cylinder. The particle tracing simulations suggest that they are therefore focused at a short distance from the exit plane of the micro-lens and diverge strongly after focus. This is consistent with the diluted beam observed on the RCF stack positioned a few cm away and in the strong dip observed in the spectrum of Fig 4 below 6 MeV. Finally, protons having very low energy (i.e. below 4 MeV in the case of Fig.4) pass through the micro-lens after the fields have vanished and do not experience any deflection.

Additional simulations were performed to test the scalability of the micro-lens to higher proton energies, as needed for applications such as proton therapy. We compute that, using the same cylinder as in our experiment and a slightly more intense CPA_2 triggering laser pulse (10^{19} W/cm^2), one could reduce the divergence of 270 MeV protons. Protons of such high energy transit through the micro-lens in a short time (13 ps), therefore even higher laser intensities, in the order of 10^{20} W/cm^2, would be required to focus them. The focusing device described in this paper has potential use in all applications of energetic protons in which reduced divergence, large flux or narrow energy range are required. These include most of the proposed applications in scientific, medical, and technological areas. For example, focusing ion beams opens new perspectives to further developments in areas such as hadron therapy for cancer treatment, accelerator physics and inertial fusion physics. Besides applications using laser-driven ion beams, such a device might find application in conventional accelerator beams as a focusing or fast switching tool.

References and notes

1. M.D. Perry and G. Mourou, *Science* **264,** 917 (1994).
2. E. Clark et al., *Phys. Rev. Lett*. **84,** 670 (2000).
3. R. Snavely et. al., *Phys. Rev. Lett.* **85**, 2945 (2000).
4. A. Maksimchuk, S. Gu, K. Flippo, D. Umstadter, V.Yu. Bychenkov, Phys. Rev. Lett. **84**, 4108 (2000).
5. V. Malka, J. Faure, Y. Glinec, A.F. Lifschitz, *Plasma Phys. Control. Fusion* **47,** B481 (2005) and references within.
6. M. Tabak et al., *Phys. Plasmas* **1,** 1626 (1994).
7. A. Rousse et al., *Phys. Rev. Lett.* **93**, 135005 (2004).
8. K.W.D. Ledingham, P. McKenna and R.P. Shinghal, *Science* **300,** 1107 (2003).
9. B.A. Remington, D. Arnet, R.P. Drake and H. Takabe, *Science* **284,** 1488 (1999).
10. M. Borghesi et al., *Phys. Rev. Lett*. **92**, 055003 (2004).
11. T. Cowan et al., *Phys. Rev. Lett*. **92**, 204801 (2004).
12. P. Patel et al., *Phys. Rev. Lett.* **91**, 125004 (2003).
13. M. Borghesi et al., *Phys. Plasmas* **9**, 2214 (2002).
14. S.V. Bulanov, T.Zh. Esirkepov, V.S. Khoroshkov, A.V. Kuznetsov, F. Pegoraro, *Phys. Lett.* A **299**, 240 (2002).

15. I. Spencer et al., *Nucl. Inst. And Meth. In Phys. Research B* **183**, 449 (2001).
16. M. Roth et al., *Phys. Rev. Lett.* **86**, 436 (2001).
17. M. Szilagyi, *Electron and ion optics* (Plenum Press, NY, 1988).
18. W. Luo, E. Fourkal, J. Li and Ch. Ma, *Med. Phys.* **32**, 794 (2005).
19. B.M. Hegelich et al., Nature **439**, 441 (2006).
20. H. Schwoerer et al., Nature **439**, 445 (2006).
21. B. Wattellier,J. Fuchs, J. P. Zou, K. Abdeli, H. Pépin, C. Haefner, *Opt. Lett.* **29**, 2494 (2004).
22. S. J. Gitomer *et al*., *Phys. Fluids* **29,** 2679 (1986).
23. M. Allen, P. Patel, A. Mackinnon, D. Price, S. Wilks, and E. Morse, *Phys. Rev. Lett.* **93,** 265004 (2004).
24. J. Fuchs *et al*., *Phys. Rev. Lett.* **94,** 045004 (2005).
25. GAFCHROMIC Radiochromic Dosimetry Films, http://www.ispcorp.com/products/dosimetry/index.html.
26. L. Romagnani et. al., *Phys. Rev. Lett.* **95**, 195001 (2005).
27. E. Lefebvre et al., *Nucl. Fusion* **43**, 629 (2003).
28. S.C. Wilks et al., *Phys. Plasmas* **8,** 542 (2001).
29. M. Key *et al*., *Phys. Plasmas* **5,** 1966 (1998).
30. These fields have been studied in detail, in planar geometry, in a previous experiment *(26)* and Fig. 3 of reference *(26)* shows their spatial and temporal evolution.
31. S. Gordienko and A. Pukhov, *Submitted to Phys. Plasmas.*
32. We acknowledge fruitful discussions with L. Gremillet, T. Grismayer, S. Gordienko, E. Lefebvre, P. Mora, A. Pukhov and V.Malka. We thank Erik Lefebvre for allowing us to use his PIC code CALDER, and the CEA/DAM for the simulations we performed on the CCRT computers. We acknowledge the expert support from the technical teams at LULI. This work has been supported by EU-Grant No. HPRICT 1999-0052, Grant No. E1127 from Région Ile-de-France, and DFG TR18 and GK1203, and partly by the QUB-IRCEP scheme and DAAD.
Correspondence and requests for materials should be addressed to Oswald Willi (e-mail: oswald.willi@laserphy.uni-duesseldorf.de)

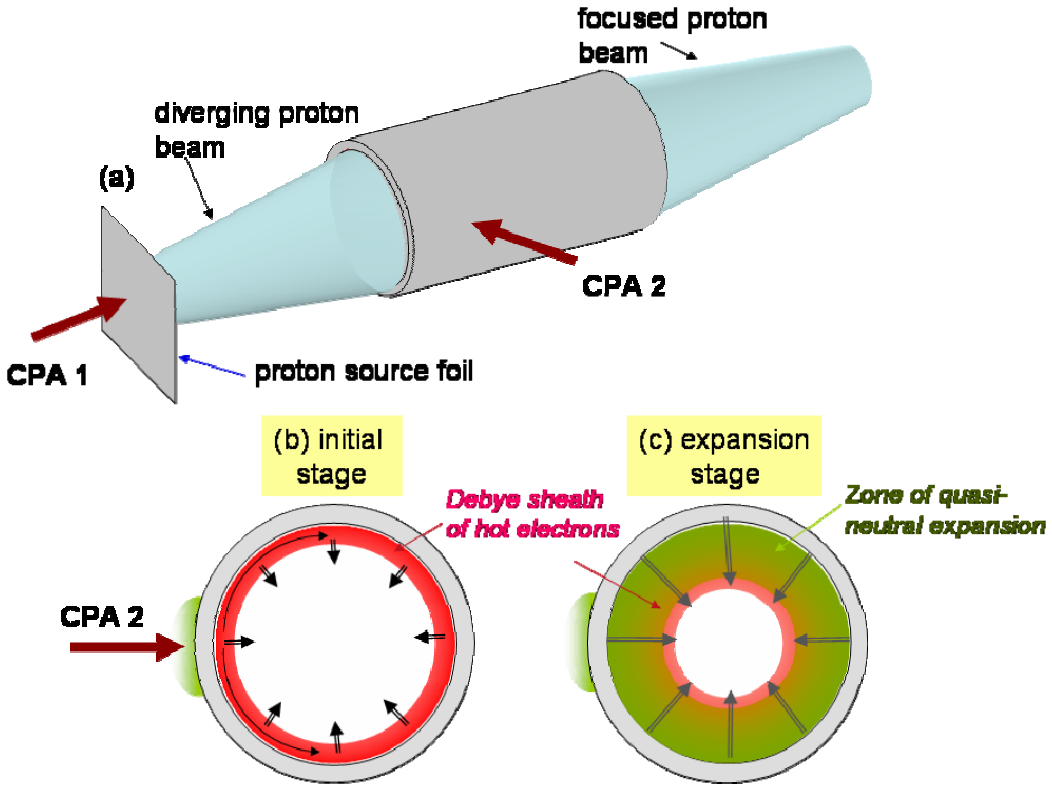

Figure 1: (A) Schematic of the micro-lens device. A proton beam is accelerated from a planar foil by the CPA_1 laser pulse. The proton beam propagates through a hollow cylinder side-irradiated by the CPA_2 laser pulse. (B,C) Schematic of the operation's principle of the micro-lens. The CPA_2 laser pulse injects hot electrons within the cylinder. These spread evenly onto the cylinder's inner wall. In the early stage (B), these electrons, confined over a Debye length over the cylinder's surface, generate a space-charge field (indicated by the radially pointing arrows), which then induces plasma expansion (C) from the cylinder's inner walls. The resulting radial electric field, still indicated by the arrows and decreasing in time as the plasma expands, focuses the protons. The field is peaked at the front but extends toward the cylinder's wall.

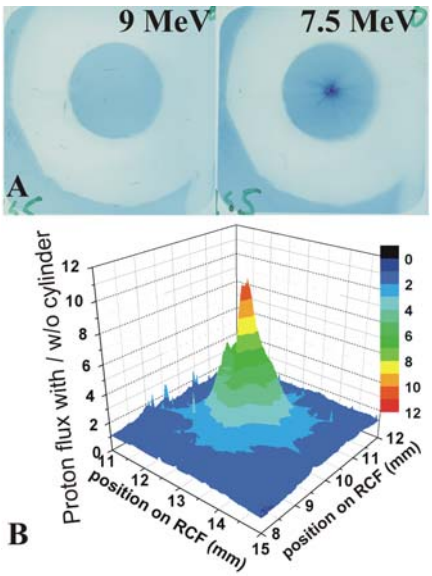

Figure 2: (A) RCF layers showing the proton beam focusing effect due to a 3 mm long, 700 µm diameter dural (95% Al, 4 % Cu and 1% Mg) laser irradiated cylinder with 50 µm wall thickness. For the energies reaching the Bragg peak in the two layers shown, the protons with an energy of 9 MeV pass through the cylinder before the electric field is present showing no focusing whereas the divergence of the protons with an energy of 7.5 MeV is strongly reduced by the electric field that has developed inside the cylinder. The shadow of the cylinder and of the 50 µm W holding wire can clearly be seen. Note that the cylinder was positioned intentionally far from the proton source in order to reduce the number of protons entering the cylinder and avoid RCF saturation. The distance between the entrance plane of the cylinder and the proton production foil was 4 mm. (B) Flux increase with respect to the unfocused flux for 7.5 MeV protons as deduced from the layer shown in (A).

c

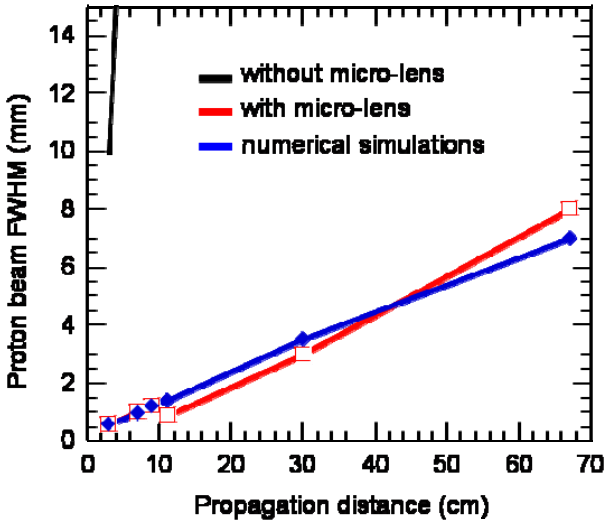

Figure 3: Evolution of the FWHM of the proton beam along its propagation, for protons with energy of 7.5 MeV (the propagation distance is calculated from the proton source). The black circles correspond to the case without micro-lens (free-space divergence), the blue diamonds to the particle tracer simulation in the fields given by the PIC simulation, and the red squares to the experimental results using the micro-lens. The RCF shown on the right-hand of Fig 2A corresponds to one of the data points in this figure.

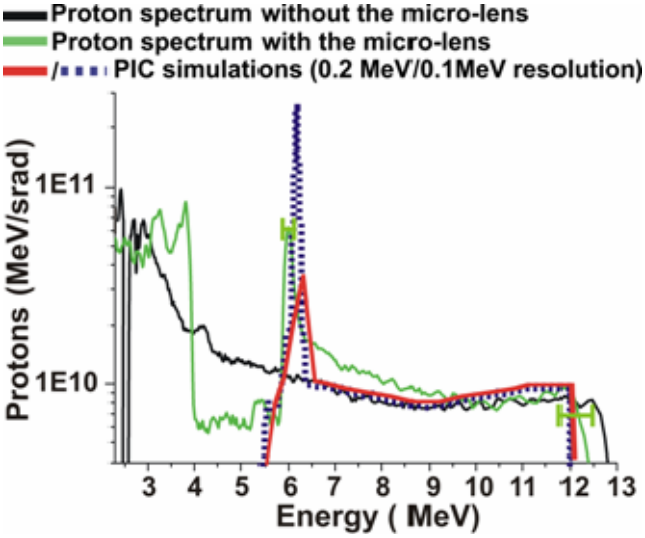

Figure 4: Experimental proton spectra measured using a magnetic spectrometer without micro-lens (black line) and with the micro-lens (green line), and proton spectrum obtained from simulations (red and blue lines) performed using the experimental proton beam parameters and the magnetic spectrometer parameters (i.e. distance from the source and slit characteristics). The red and blue curves are obtained using energy bins of 0.2 and 0.1 MeV, respectively. The simulated spectrum was obtained by tracing, for each energy bin, 5000 protons through the fields predicted by the PIC simulation.